Adhesive Dynamics Simulation of G-Protein-Mediated Chemokine-Activated Neutrophil Adhesion

Kelly E. Caputo[†] and Daniel A. Hammer[‡*]
[†]Department of Chemical and Biomolecular Engineering and [‡]Bioengineering, University of Pennsylvania, Philadelphia, Pennsylvania 19104

ABSTRACT To reach sites of inflammation, a blood-borne neutrophil first rolls over the vessel wall, becoming firmly adherent on activation, and then transmigrates through the endothelium. In this study, we simulate the transition to firm adhesion via chemokine-induced integrin activation. To recreate the transition from rolling to firm adhesion, we use an integrated signaling adhesive dynamics simulation that includes selectin, integrin, and chemokine interactions between the cell and an adhesive substrate. Integrin bonds are of low affinity until activated by chemokine binding to G-protein coupled receptors on the model cell. The signal propagates within the cell through probabilistic diffusion and reaction of the signaling elements to induce the high-affinity integrins required for firm adhesion. This model showed that integrins become progressively active as cells roll and interact with chemokines, leading to a slight slowing before firm adhesion on a timescale similar to that observed in experiments. Increasing the density of chemokine resulted in decreases in the rolling time before stopping, consistent with experimental observations. However, a limit is reached where further increases in chemokine density do not increase adhesion. We found that the timescale for integrin activation correlated with the time to stop. Further, altering parameters within the intracellular signaling cascade that changed the speed of integrin activation, such as effector activation and dissociation rates, correspondingly affected the time to firm adhesion. For all conditions tested, the number of active integrin bonds at the point of firm adhesion was relatively constant. The model predicts that the time to stop would be relatively independent of selectin or integrin density, but strongly dependent on the shear rate because higher shear rates limit the intrinsic activation rate of integrins and require more integrins for adhesion.

INTRODUCTION

At sites of inflammation in the body, neutrophils flowing in the blood stream are captured by selectin adhesion molecules upregulated on inflamed endothelium and begin to roll. After a period of selectin-mediated rolling, the cells stop and firmly adhere to the vessel wall, followed by extravasation to the unhealthy tissue via morphological changes and crawling through the endothelium. Firm adhesion at an inflammatory site, mediated by activation of the integrin lymphocyte function-associated antigen-1 (LFA-1) (1), is an essential step in this process.

LFA-1 and other β_2-integrins bind to intracellular adhesion molecule-1 (ICAM-1). Under resting conditions, wild-type LFA-1 is predominantly in a low-affinity state, but a higher-affinity state is required for firm adhesion (2–4). The change to a high-affinity state is believed to require a conformational change; integrin $\alpha_V\beta_3$ has been visualized by electron microscopy with various degrees of extension, a characteristic likely also exhibited by LFA-1 (5,6). Furthermore, the I-domain fragment of LFA-1, which binds ICAM-1, can adopt different conformations and affinities for binding ICAM-1 (7,8). Thus, integrins can modulate their affinity during inflammation. To study firm adhesion in vitro, experimentalists have activated integrins by the addition of cations (9,10), mutations in the I-domain that lock it in a given conformation (11), or binding it with activating antibodies (12).

In vivo, integrins are activated by outside-in signaling through selectins (13) or exposure to inflammatory chemokines (14,15). Many in vitro experiments have been carried out in flow chambers to study cell activation by chemokines. Sometimes, a soluble chemokine is applied in the fluid-phase and, generally, these cells are rapidly activated before adhesion under flow (16,17). In other experiments, chemokine molecules may be immobilized on the adhesive surface to which the cells subsequently adhere (14,15,18) or expressed on cultured endothelial cells stimulated to mimic inflammatory conditions (19–21). In these experiments, leukocytes are activated, but the speed of activation and firm adhesion seems to differ with the cell type, the densities of chemokine and adhesion molecules, and the flow rate. For example, DiVietro et al. (18) have recreated the transition from rolling to firm adhesion in a flow chamber. They coated the reactive surface with P-selectin, the integrin ligand ICAM-1, and the chemokine interleukin-8 (IL-8), and showed that neutrophils rolled and then slowed to a stop on this minimal surface, reporting how the time to stop decreases as a function of increasing chemokine density. They showed the timescale of neutrophil activation could decrease from 117 to 30 s when the density of IL-8 increased from 60 to 350 sites/μm^2 on a surface that also contained P-selectin and ICAM-1.

Our goal is to develop a calculus to predict the activation and adhesion by leukocytes in response to immobilized chemokine. In this study, we modify the adhesive dynamics model developed previously in our lab (22–25) to study the initial firm adhesion of a neutrophil after a period of rolling.

Submitted May 20, 2008, and accepted for publication December 5, 2008.

*Correspondence: hammer@seas.upenn.edu

Editor: Jason M. Haugh.

0006-3495/09/04/2989/16 $2.00

doi: 10.1016/j.bpj.2008.12.3930

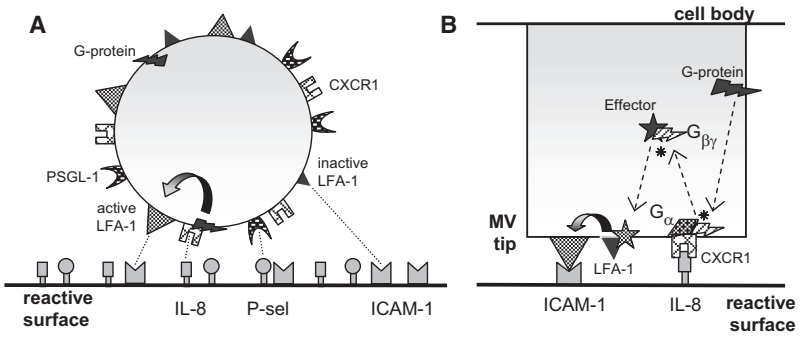

FIGURE 1 Model schematics. (*A*) The interactions important to the Adhesive Dynamics module are shown. The reactive surface displays three molecules that can bind to cell-surface molecules. In the model, the cell-surface molecules are on the tips of cylindrical protrusions that can stretch like microvilli, but here, the cell is depicted without microvilli for clarity. PSGL-1 on the cell binds to P-selectin on the reactive surface whereas CXCR1 binds to IL-8. A signaling cascade (*B*) can lead to activation of LFA-1 on the cell. Both inactive and active LFA-1 can bind to ICAM-1 on the surface, but the active form has a higher affinity. (*B*) The steps in the signaling module are demonstrated. Transmembrane G-protein molecules in a microvillus can diffuse and bind to CXCR1 at the microvillus tip. When CXCR1 is bound to IL-8 extracellularly, the associated G-protein can become active, dividing into two subunits, α and $\beta\gamma$, that can then diffuse within the membrane. The $\beta\gamma$ subunit can bind with a diffusing Effector molecule and activate it. The active Effector can then diffuse and bind to the intracellular portion of LFA-1, thereby activating it.

Adhesive dynamics is a mechanically rigorous dynamic simulation of cell adhesion that models adhesion molecules as reactive springs. The motion and adhesion of a cell results from a force and torque balance. Bond formation and force-driven breakage are calculated by random number sampling of probability functions. This method has calculated the rolling of leukocytes (23,24,26–29), the detachment of cells from surfaces (30,31), and the firm adhesion of leukocytes (23,24). Recently, we developed a class of simulation referred to as integrated signaling adhesive dynamics (ISAD), where signaling pathways and adhesion are interconnected. A version of ISAD was reported in which a mitogen-activated protein kinase (MAPK) pathway initiated by selectin ligation resulted in integrin activation and, consequently, a transition from rolling to firm adhesion (25,32). However, we currently believe that chemokine ligation is the predominant mechanism of adhesion in leukocyte systems—including neutrophils and lymphocytes—and now we turn our attention to this important pathway.

In this study, we extend our ISAD method to simulate leukocyte stopping via a chemokine receptor. We include a G-protein coupled receptor (CXCR1) on the cell that, when bound to IL-8, can initiate G-protein activation (17,33). Further, we have embedded a G-protein signaling network within the cell that allows us to couple chemokine ligation to the dynamics and extent of integrin activation. With this ISAD simulation, we recreate the transition from rolling to firm adhesion on a timescale similar to that observed by DiVietro et al. (18). We also predict a dependence of the activation rate on IL-8 surface density consistent with that seen experimentally. Furthermore, we explore the effect of various rates within the signaling cascade on the speed of signal propagation and time for leukocyte homing. Finally we make predictions about the effect of ligand density, flow rate, and pharmacological treatment of G-proteins to precouple G-protein molecules with CXCR1. The result is a comprehensive model of leukocyte firm adhesion through chemokine activation that is consistent with experiment and provides numerous testable predictions.

MODEL

The model used to study the transition of a neutrophil from rolling to firm adhesion is similar to previous adhesive dynamics models where the cell is treated as a hard sphere with extensible cylindrical protrusions representing the microvilli. The basic details of cell motion and stochastic bond association and dissociation can be found in previous work (22–24,27,32). Note that the microvilli in this model are allowed to elastically deform, but are not allowed to enter the tether regime (27). This provides the effect of more robust rolling due to microvillus extension without adding the relative complexity of the tether regime, which is unnecessary in this study because simulations are focused on the signaling step of the adhesion cascade.

Adhesion module

As in other adhesive dynamics models of cell rolling, the cells have adhesion molecules located on the tips of their microvilli so they are able to access the uniformly adhesive surface over which the cells flow. An illustration of the adhesion molecules can be seen in Fig. 1 *A*. Initially, P-selectin glycoprotein ligand-1 (PSGL-1) on the cell surface mediates rolling by binding P-selectin. The molecular pair responsible for firm adhesion is the integrin LFA-1 on the cell and ICAM-1 on the reactive surface. The integrin exists in its resting, inactive state with a low binding affinity for ICAM-1 until it becomes activated through the signaling cascade (7). The high affinity binding of the active LFA-1/ICAM-1 bond is responsible for firm adhesion of the model cell. Finally, the interaction of a third molecular pair is included. The chemokine receptor, CXCR1 is located on the cell and can bind to the chemokine IL-8 on the reactive surface. It is this interaction that initiates the signaling cascade, leading to activation of the integrins. The number of receptors on a microvillus tip is based on published reports (PSGL-1) (27,34–37) or is estimated from the measured total number of receptors on the cell assuming a uniform distribution (13,33,38,39).

TABLE 1 Adhesion module parameters

Adhesion pair	k_{on}^0 * [$\mu m^2/s$]	Dissociation rate k [s^{-1}]; f [pN]; γ [Å]	λ [nm]	σ [pN/nm]	ρ_{ligand} [No./μm^2]	ρ_{recept} [No./MV]
PSGL-1/P-selectin	1.7	$k_{1rup} = 10$; $k_2^0 = 0.37$; $f_\beta = 18$; $\Phi_0 = 100$; $f_{12} = 5$	70	5	60	3
Resting LFA-1/ICAM-1	0.3	$k_r^0 = 4$; $\gamma = 1.5$	24	50	50	3
Active LFA-1/ICAM-1	100	$k_{r,1}^0 = 0.17$; $\gamma_1 = 2.1$ $k_{r,2}^0 = 40$; $\gamma_2 = 0.24$	44	50	50	0
CXCR1/IL-8	0.002	$k_r^0 = 0.1$; $\gamma = 25$	18	5	220	1

*Association rates are approximated from previous work (79,80) and a large affinity increase from resting to active integrin (7). The chemokine association rate is unknown and the value gave relatively good agreement with experimental stop times.

Each of the four possible interactions (PSGL-1/P-selectin, resting LFA-1/ICAM-1, active LFA-1/ICAM-1, and CXCR1/IL-8) in the adhesion module is described by its own set of reaction rate parameters, which are given in Table 1. All of the association rates depend on the relative motion of the binding surfaces as described by Chang and Hammer (40). A simple linear increase in association rate with Peclet number (Pe) is assumed in this study, which is a good approximation at low shear rates that we use. The unstressed association rate is given by the following equations in the diffusion and convection limits:

$$k_{f\,diff}^0 = k_{on}^0 \frac{\rho_{ligand}}{\ln(b/a)} \quad (1)$$

$$k_{f\,conv}^0 = k_{on}^0 \mathrm{Pe} \rho_{ligand}. \quad (2)$$

In these expressions, k_{on}^0 is an unstressed association rate on a per ligand density basis and is corrected for the appropriate encounter rate by incorporation in Eq. 1 or 2. The ligand density on the adhesive surface is given by ρ_{ligand}, b is the average distance between ligand molecules, and a is the reactive radius for the receptor. At low shear rates, $\mathrm{Pe} = |V|a/D$, where $|V|$ is the relative velocity between the two binding surfaces and D is the relative diffusion constant of the binding molecules, is small. Diffusive encounter dominates over convective encounter and Eq. 1 is used. When Pe increases such that convection dominates, Eq. 2 is used to determine the unstressed association rate.

As in previous models, the unstressed association rate, k_f^0, is corrected for deviation of the potential new bond from the ideal bond length to maintain a Boltzmann distribution (41):

$$k_f = k_f^0 \frac{k_r}{k_r^0} \exp\left[\frac{-E_{bond}}{k_B T}\right]. \quad (3)$$

Here, k_r and k_r^0 are the stressed and unstressed dissociation rates, respectively, E_{bond} is the potential energy of the bond, and $k_B T$ is the thermal energy. Assuming the bond acts as a Hookean spring in extension with spring constant σ and equilibrium length λ, $E_{bond} = 1/2\ \sigma\ (z\text{-}\lambda)^2$ is the potential energy of an extended bond of length z. However, in compression, we assume $E_{bond} = 0$ up to a cutoff point. It is assumed that bonds experience no force up to this point, but cannot exist compressed beyond it where the potential energy becomes infinite. In atomic force microscopy experiments, Marshall et al. (42) observed a ''dead zone'' during which no force is required to extend a bound pair of molecules, supporting this assumption. Each interacting pair has unique Hookean spring parameters (Table 1) with λ equal to the sum of the molecular lengths (20,43–46) and σ consistent with measured values (42,43).

The dissociation rate models are different for different bonds according to our accumulated detailed understanding of molecular dissociation of these molecules elucidated with molecular spectroscopy. The Bell model (47), which describes an exponential increase in off rate with force, fits with experimental data well. The dissociation rate, k_r, according to this model is:

$$k_r = k_r^o \exp\left[\frac{\gamma f}{k_B T}\right], \quad (4)$$

where γ is the reactive compliance and f is the force on the bond. The Bell model was chosen to describe the dissociation of CXCR1/IL-8, which has not been well-studied mechanically. It has been noted, however, that it cannot readily withstand force (18), so the reactive compliance for this signaling bond is very large, leading to fast dissociation at relatively low forces.

Based on single-molecule atomic force microscopy experiments (48), both the inactive and active LFA-1/ICAM-1 bonds have two activation barriers for breakage. Each activation barrier has its own set of Bell model parameters, and the overall time for dissociation (the inverse of the rate of dissociation) is simply equal to the sum of the times for dissociation over each barrier. The parameters for the two barriers to active integrin bond dissociation are from Zhang et al. (48). For simplicity, the Bell model was chosen to describe the resting LFA-1/ICAM-1 bond because it provides a straightforward model appropriate for its small role in adhesion. The parameters for the resting integrin bond were taken to be those for the outer barrier in the two-barrier dissociation rate (48).

The dissociation rate for the P-selectin/PSGL-1 bond has been shown to first decrease, then increase, with force. The model and parameters for this catch-slip selectin bond are given by Evans et al. (49). The bond is assumed to exist in one of two possible states. Dissociation from state 1 is fast, whereas that from state 2 is slower. Furthermore, state 1 is of lower energy at zero force and is therefore highly occupied at low forces. However, state 2 becomes preferentially occupied at higher forces. This model is described by (49):

$$k_r = \frac{\Phi_0 k_{1rup} + \exp\left(\frac{f}{f_{12}}\right)\left[k_2^0 \exp\left(\frac{f}{f_\beta}\right)\right]}{\Phi_0 + \exp\left(\frac{f}{f_{12}}\right)}, \quad (5)$$

where $\Phi_0 = \exp(\Delta E_{21}/k_B T)$ is the equilibrium constant between the two states at zero force when the energy difference is ΔE_{21}. The constant dissociation rate from state 1 is k_{1rup}, whereas, for state 2, k_2^0 is the unstressed dissociation rate and f_β is the thermal energy divided by the reactive compliance. Finally, f_{12} is the force scale for the shift in equilibrium state occupancy as a function of force on the bond.

Signaling module

As discussed, there are integrin molecules located on the surface of the cell that can bind to their ligand ICAM-1 on the reactive surface. At the beginning of the simulations, LFA-1 exists in its resting state, but, through signaling, it can be activated to the high-affinity state responsible for firm adhesion of the cell. The model for signaling is described in this study and depicted in Fig. 1 *B*.

Although there has been a great deal of research to determine the players in leukocyte activation, the signaling cascade is not completely understood (50), especially for the initial activation leading to firm adhesion. We have therefore rendered the G-protein signaling network into a simple yet reasonable pathway. It is known that chemokines bind to G-protein coupled receptors (GPCRs) on the cell, activating the G-protein (13), so our model begins there.

The chemokine IL-8 on the reactive surface can bind to CXCR1, the GPCR on the cell surface, located on the microvillus tips in this model. At the same time, G-proteins inside the cell can diffuse and bind to the intracellular portion of CXCR1. When IL-8 is bound to the extracellular portion, CXCR1 is activated and can then in turn activate a coupled G-protein. On activation, the G-protein splits into two active subunits, G_α and $G_{\beta\gamma}$. Each of the subunits can diffuse in the membrane. It is assumed that the $G_{\beta\gamma}$ subunit acts to propagate the signal in this case (51–53). Because the remainder of the signaling process is likely complicated and not definitively known for granulocytes, we simplify it by saying that a small cytoplasmic molecule called the Effector acts as the intermediate between G-protein activation and LFA-1 activation. Recent evidence in lymphocytes suggests the key effector is Rap1 (54,55), but a different molecule may play the role in granulocytes.

The Effector can receive the $G_{\beta\gamma}$ signal by diffusing into contact, binding, and then becoming active. The Effector can then diffuse to a resting LFA-1 molecule and bind to its intracellular portion, thereby affecting a conformational change that activates the integrin. When the Effector dissociates from an active LFA-1 molecule, the integrin may relax back to its resting state. Meanwhile, the free and active G_α subunit may become inactive, allowing it to rebind with the $G_{\beta\gamma}$ subunit, reforming the inactive G-protein. This is similar to how Rap1 works in lymphocyte systems.

This signaling process can occur independently in each microvillus and is assumed to take place on a one-dimensional lattice, with 1000 rungs along the length of the 0.3 μm-long microvillus. Each microvillus contains 5 G-proteins and 5 Effectors, and these mobile elements are randomly assigned a starting position on the lattice. Other signaling elements that are also involved in adhesion are in a fixed position at the bottom of the lattice, representing the microvillus tip. Essentially, we are looking at local integrin activation rather than global activation due to the restriction to independent microvilli. We believe this is likely what happens at short times after exposure to endothelium-expressed chemokines (50), and future versions of this integrated model may be created that allow longer length and timescale signal transduction.

The diffusion and reaction steps in the signaling module occur at every time step, $\Delta t = 10^{-7}$ s, within the ISAD algorithm. The signaling module begins by allowing all mobile elements to diffuse by randomly choosing a direction for their motion. The hop size, Δx, for a particular element along the lattice is determined by the diffusion constant, D, of that element and the time step of the simulation as follows:

$$D = \frac{(\Delta x)^2}{2\Delta t}. \quad (6)$$

Because the G-protein and its subunits are assumed to be membrane-bound, their hop size of one rung is smaller than the 10-rung hop size of the cytoplasmic Effector molecule. These hop sizes give diffusion coefficients of 0.45 and 45 $\mu m^2/s$.

After the diffusion step, each signaling element is allowed the possibility to react with nearby elements. This possibility is calculated from random number sampling of reaction probabilities. If the signaling element is already bound to another, the possible reactions include i), dissociation, and ii), catalytic spin flip (25), where the presence of one active element increases the rate at which the inactive element becomes active. If the element is not bound, it may i), associate with an unbound element that is within reactive distance (10 rungs), or ii), undergo an auto spin flip, where an active molecule switches back to its inactive state.

The rate, k, of each possible reaction, i, is given in Table 2 for the base case. Association rates are the intrinsic reaction rate for a molecular pair that has already encountered by diffusion, and are fast because reactions are assumed to be diffusion limited (56). Other rates are based on previous signaling models (57,58). Unknown Effector rates are assumed to be of the magnitude of similar reactions and will be explored. The probability, P, that a reaction will occur during a given time step is:

$$P_i = 1 - \exp(-k_i \Delta t). \quad (7)$$

The probability that a particular element will have no reaction is simply the product of the probabilities that each possible reaction will not occur, $\prod_i (1 - P_i)$. Therefore, the probability that some reaction will occur for a particular element is:

TABLE 2 Signaling module base case reaction rates

Reaction*	Rates:† Association	Dissociation	(Auto) Spin flip
$C + G \underset{10}{\overset{1}{\rightleftarrows}} CG$	1×10^4	0.03	—
$C^* + G \underset{11}{\overset{2}{\rightleftarrows}} C^*G$	1×10^6	0.01	—
$C^*G \xrightarrow{16} C^* + Ga^* + Gbg$	—	—	5.0
$Gbg + E \underset{12}{\overset{4}{\rightleftarrows}} GbgE$	5×10^5	0.1	—
$GbgE \xrightarrow{17} GbgE^*$	—	—	10.0
$GbgE^* \underset{5}{\overset{13}{\rightleftarrows}} Gbg + E^*$	1×10^5	0.1	—
$I + E^* \xrightarrow{8} I^*E^*$	1×10^6	—	—
$I^*E^* \underset{6}{\overset{14}{\rightleftarrows}} I^* + E^*$	1×10^6	0.1	—
$LI + E^* \xrightarrow{9} LI^*E^*$	1×10^6	—	—
$LI^*E^* \underset{7}{\overset{15}{\rightleftarrows}} LI^* + E^*$	1×10^6	0.1	—
$I^* \xrightarrow{20} I$	—	—	1.0
$LI^* \xrightarrow{21} LI$	—	—	0.01
$E^* \xrightarrow{19} E$	—	—	1.0
$Ga^* \xrightarrow{18} Ga$	—	—	0.1
$Ga + Gbg \xrightarrow{3} G$	1×10^6	—	—

*Signaling elements are abbreviated as follows: C, CXCR1; G, G-protein; Ga, G_α; Gbg, $G_{\beta\gamma}$; E, Effector; I, LFA-1; LI, ligand-bound LFA-1. When two symbols are written together, they are bound. A star signifies an active element as opposed to the inactive form.

†All reaction rates are given in units of s^{-1}. Association rates are the intrinsic reaction rate of a molecular pair that has already encountered by diffusion.

$$P_{\text{rxn}} = 1 - \exp(-k_{\text{tot}}\Delta t), \tag{8}$$

where $k_{\text{tot}} = \sum_i k_i$ is the sum of the rates of all possible reactions for a particular element. If a reaction indeed happens according to Monte Carlo sampling, it is assumed that only one reaction occurs during the time step. The reaction that occurs is chosen randomly based on the individual reaction rates compared to the total, with faster reactions more likely to occur.

Aside from obvious differences in the identities of the signaling components, our implementation of the signaling algorithm differs somewhat from that used in previous work from our lab (25). The basic idea of stochastic diffusion of signaling elements and reaction on collision is the same. However, instead of calculating probabilities based on activation energies as before (25), we now use reaction rates so that the signaling and adhesion modules take similar approaches. Kruk et al. (59) used an algorithm similar to this signaling algorithm in a study of the dynamics of central synapses. In addition, this model includes deformable microvilli, which permit smaller, more realistic numbers of adhesion molecules on the cell surface while still providing significant adhesion. Also, adhesion molecules in this model have different bond lengths and spring constants. The increase in length experienced by an activating LFA-1 molecule is included as well.

Computation

Simulations were programmed in C++ using Microsoft Visual C++ 6.0 and run on a Dell Precision Workstation with 3.06 GHz Intel Xeon processors. Simulations began with the cell in binding proximity to the adhesive surface and exposed to a shear flow. Adhesion and signaling molecules were immediately allowed to interact according to the algorithm described above. Cell center and microvillus positions, along with bonding data, were recorded every 0.1 s. Results were visualized with MATLAB 6.5 (The MathWorks, Natick, MA).

RESULTS

The ISAD model was used to simulate a neutrophil as it rolls and then stops on a surface displaying a set of molecules at an inflammatory site at a shear rate of 100 s^{-1}, unless indicated otherwise. In the results that follow, a cell was considered stopped and the simulation was ended when it progressed less than half of a cell diameter in 10 s. At each set of parameters examined, the simulation was run six to nine times and the results averaged. Error bars represent the standard error.

Basic results

First, we simulate an experiment in which neutrophils are convected over a surface coated in adhesion molecules and chemokines, and ultimately roll and stop. As in the experiments by DiVietro et al. (18), we use P-selectin, ICAM-1, and IL-8 as the surface molecules to provide rolling, firm binding, and signal initiation, respectively. We found that the model cells indeed rolled and came to a stop, as seen in the sample trajectories in Fig. 2 *A* for an IL-8 density of 220 sites/μm^2, which corresponds to one of the densities used by DiVietro et al. (18). In this simulation, as in the experiment (18), the densities of P-selectin and ICAM-1 were 60 and 50 sites/μm^2, respectively. Most of the simulated trajectories have some longer pauses as the cell approaches firm adhesion due to the emergence of a small number of active integrin bonds. This slowing before stopping was also noted in experiments (18).

For the cell whose trajectory is highlighted in gray (Fig. 2 *A*), several quantities calculated during the simulation are presented in Fig. 2, *B–I*, as a function of time. The velocity gradually decreases as the cell becomes active and comes to a stop (Fig. 2 *B*). The longer pauses correspond to times when microvilli with active integrins are bound (Fig. 2, *C* and *D*). The numbers of chemokine, selectin, and resting LFA-1 bonds fluctuate through the simulation, but show less fluctuation once the cell stops and the microvilli in the contact area do not change (Fig. 2, *E–G*). We observed a gradual increase in the number of active integrin molecules on the cell (Fig. 2 *C*). The first integrin was activated after

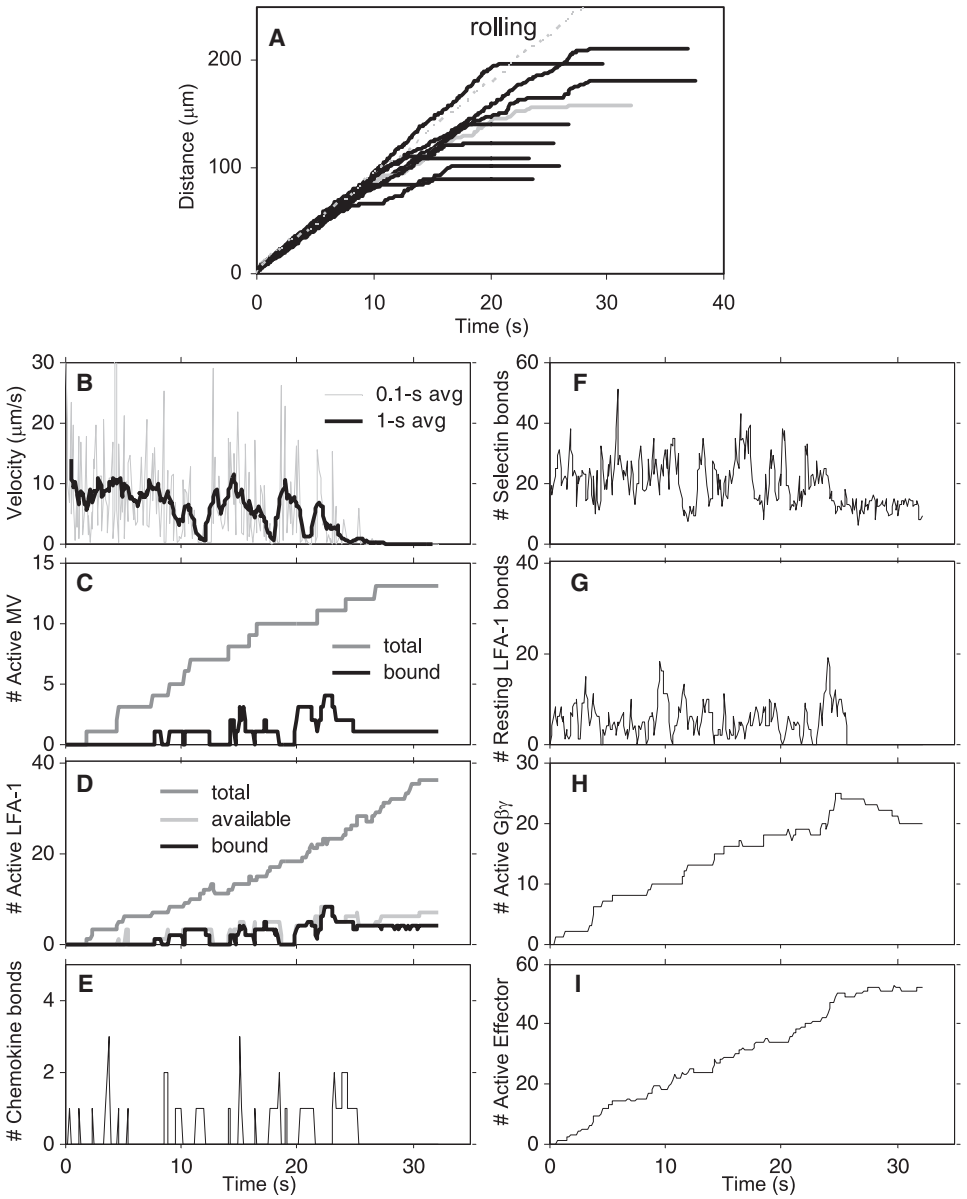

FIGURE 2 Example results for activation leading to firm adhesion. (*A*) Several trajectories are shown depicting the slowing and stopping of simulated cells as they become active. All trajectories are for an IL-8 density of 220 sites/μm^2 and base case parameters, but with different random number seeds. The trajectory of a rolling cell that is not allowed to become active is indicated by a gray dashed line for comparison. Several quantities calculated during the simulation are shown in (*B–I*) for the cell with the gray trajectory. (*B*) Velocity as a function of time. Both the backward 0.1-s average velocity and centered 1-s average velocity are shown. The cell slows and has longer pauses as it rolls. (*C*) Number of microvilli with active integrins. The total number of active microvilli gradually increases as the cell accumulates signal, but the number of active microvilli bound at the time of firm adhesion is small. (*D*) Number of active integrins on the cell, available to bind in the contact area, and bound. About 2 s go by before any LFA-1 becomes active, and then the total gradually increases. A majority of those active integrins near enough to bind to the surface are bound. (*E*) Number of chemokine bonds. This number fluctuates but remains small. (*F*) Number of selectin bonds. (*G*) Number of resting LFA-1 bonds. (*H*) Number of active $G_{\beta\gamma}$ in the cell. G-proteins become active quickly and the number gradually increases. There are some decreases because G_α can deactivate and recombine with $G_{\beta\gamma}$. (*I*) Number of active Effector molecules in the cell.

about 2 s of rolling, during which the initial steps in the signaling cascade occurred. We refer to this as the ''time to first activation'' and this time varies from cell to cell due to the stochastic nature of the simulation and according to parameter values. With the parameter values used here, the LFA-1 that becomes active is not immediately available to bind because the microvillus may rotate out of the contact zone before activation occurs. However, once the active LFA-1 molecules reenter the contact zone, they rapidly bind. As mentioned, the signaling cascade is active before the first integrin becomes active. The small number of chemokine bonds is sufficient to quickly initiate signal transduction, as indicated by active $G_{\beta\gamma}$ and Effector molecules at early time points (Fig. 2, *H* and *I*). The quantities of both of these intracellular signaling molecules increase as the cell rolls and accumulates IL-8 signal, becoming active.

Effect of IL-8 density

Prompted by the study by DiVietro et al. (18), we looked at the effect of varying IL-8 density on the transition to firm adhesion. Fig. 3 *A* shows good agreement between the distances rolled before stopping in simulations and in experiments, with increasing distance to stop as the IL-8 density decreases (18). In Fig. 3 *B*, both the time and distance rolled in the simulations before stopping are presented. At very high IL-8 densities, the time to stop approaches a minimum because the time the chemokine signal takes to propagate through the cell to activate the integrins becomes rate-limiting. If no IL-8 were present, cells would continue to roll and never stop as no signal would be initiated. Because cells have an average velocity that does not significantly vary with IL-8 density, the distance the cells roll before stopping

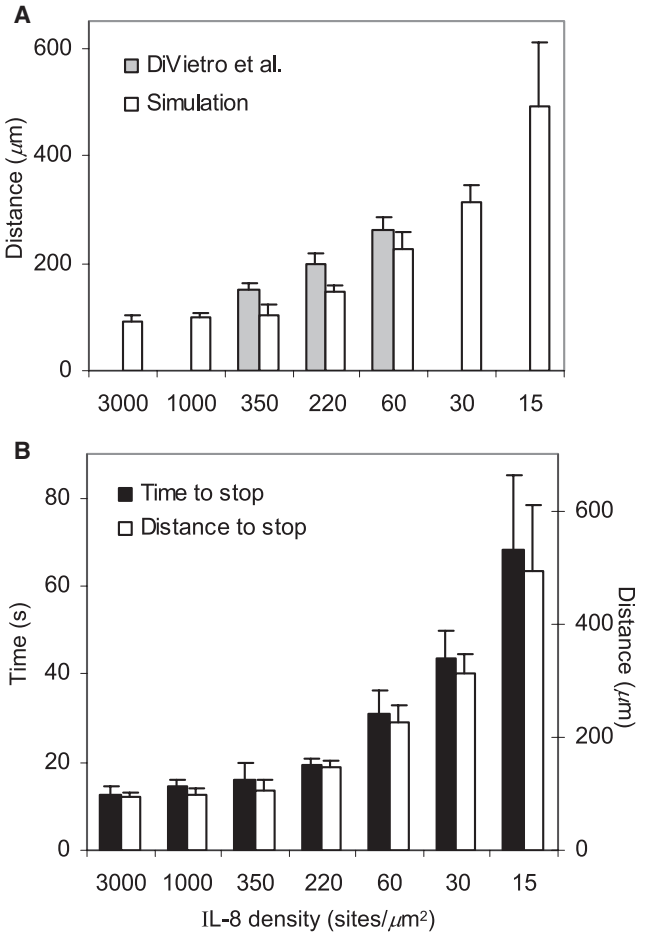

FIGURE 3 Effect of IL-8 density on time and distance rolled before firm adhesion. (*A*) Distance rolled before firm adhesion at various IL-8 densities. For comparison, distances from DiVietro et al. (18) are shown with the simulation results. (*B*) Time and distance to stop in simulations at the indicated IL-8 densities. Cells flowing over a surface with a higher chemokine density achieve firm adhesion more quickly than those exposed to lower chemokine densities. The time and distance to stop approach a minimum at the highest IL-8 densities tested.

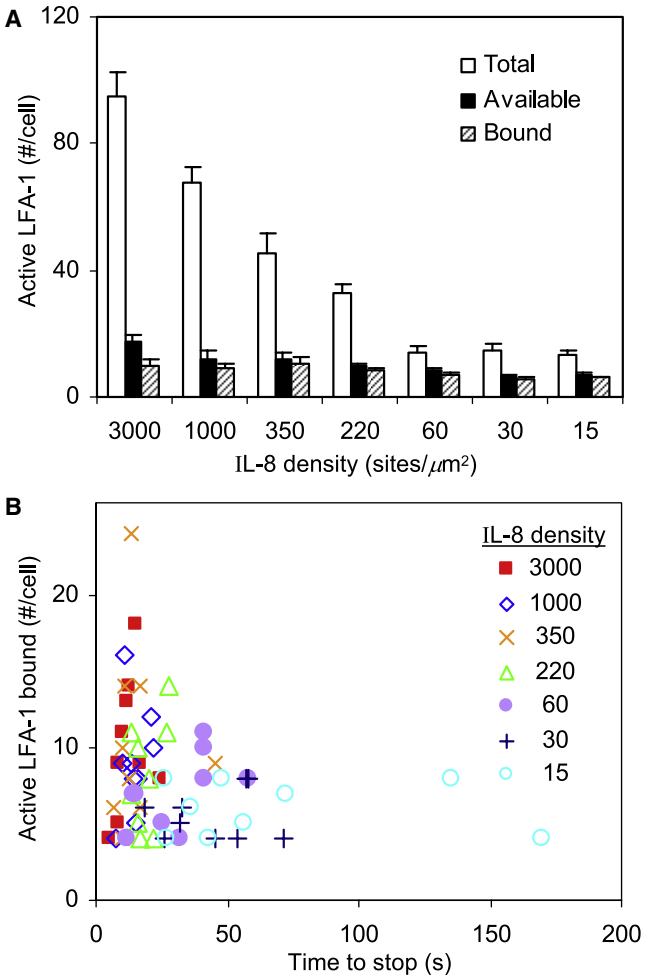

FIGURE 4 Number of active integrins present at the point of firm binding for various chemokine densities. (*A*) Average number of active LFA-1 molecules on the entire cell, within the contact area, and bound to their ligand ICAM-1 at the end of the simulation for each IL-8 density. The total number of active integrins on the cell clearly decreases with IL-8 density. But, the number with the potential to bind and the number bound at the stoppage point remain relatively constant. (*B*) Number of active integrins bound when the cell is firmly adherent as a function of time to stop for each run. Runs at the same IL-8 density are given by the same symbol. No cell stops with fewer than 4 active integrin molecules bound, but cells exposed to higher IL-8 densities are more likely to stop with more active integrins bound.

corresponds to the time they take to stop. However, as noted in Fig. 2, the cells roll more quickly at first and slow as integrin molecules become active before coming to a stop. Thus, velocity decreases as cells roll on an IL-8 substrate.

The number of active LFA-1 molecules present during rolling and activation is explored in Fig. 4 *A*. At the time of arrest, there are more active integrins on the whole cell when the cell is exposed to a surface with a high IL-8 density. Interestingly, the number of active LFA-1 molecules that are in the contact area and the number that are bound to ICAM-1 when the cell comes to a stop are relatively constant for all chemokine densities. We hypothesize that firm arrest only requires a small number of ligated active LFA-1, as determined by the mechanics of adhesion, even though there could be widespread LFA-1 activation over the cell. In Fig. 4 *B*, we illustrate the number of active LFA-1 engaged and the corresponding time to stop. Apparently, there is a minimum number of active LFA-1 bonds required for a cell to stop. This is dictated by the mechanics of adhesion. At each IL-8 density tested, cells will stop once the minimum number of active integrin bonds is surpassed, but cells exposed to higher densities of chemokine are more likely to come to arrest with a larger number of active integrin bonds. At high IL-8 densities, integrins are rapidly activated. The number of active integrins (Fig. 4 *A*) is high and the number of ligated active integrins is greater than the minimum required for arrest. This is because the integrin activation rate exceeds the adhesion rate, leading to more integrin activation than required for adhesion. At low IL-8 densities, cells ultimately come to a stop with the minimum number of active LFA-1 bonds needed for adhesion,

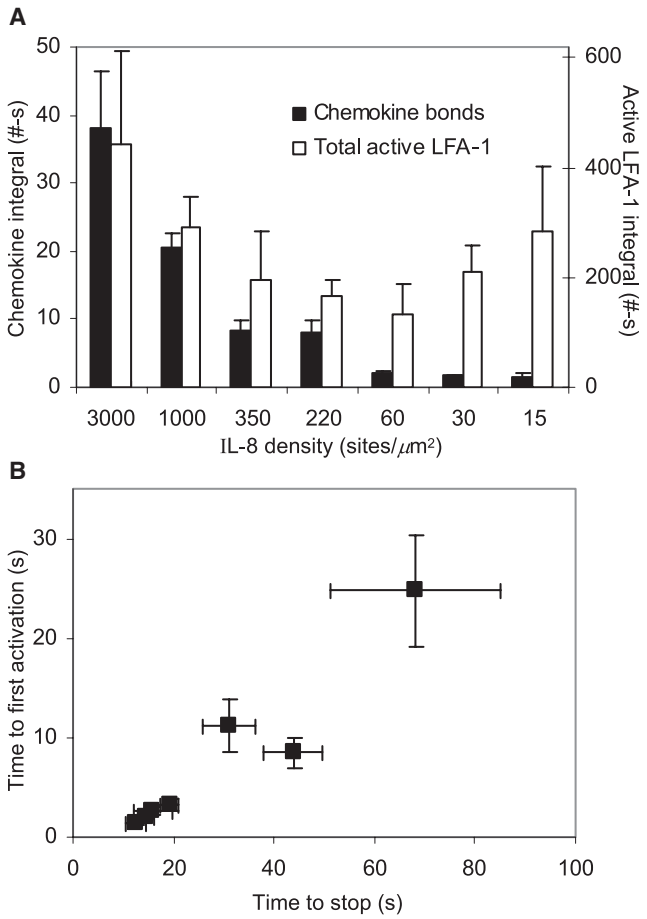

FIGURE 5 Integrals over rolling time and the characteristic activation time. (*A*) Average value of the number of chemokine bonds and number of active integrin molecules on the cell integrated over the rolling time for each IL-8 density. The chemokine integral is smaller for smaller values of the IL-8 density whereas the active integrin integral shows a minimum. (*B*) The average time to the first integrin activation as a function of the average time to stop plotted for each IL-8 density. The average time to stop correlates well with this measure of a characteristic activation time.

although it takes a longer time for these adhesion molecules to accumulate and for the cell to stop (Fig. 4 *B*).

Both the number of active LFA-1 molecules on the cell and the amount of time an activating cell is exposed to the adhesive surface contribute to the time it takes to stop, so it is interesting to examine the integrals of activity over time. Fig. 5 *A* reports the values of the integral of the active integrins on the cell and the integral of chemokine bonds over the rolling time of the cells. The integral of chemokine bonds clearly decreases with decreasing IL-8 density. At the lower chemokine densities, there is less IL-8 available to bind. As the chemokine density decreases, the cell rolls further, but because chemokine density is lower, the integral of chemokine bonds goes down. The integral of active LFA-1 over the rolling time, surprisingly, goes through a minimum with IL-8 density (Fig. 5 *A*). A possible explanation is that at high IL-8 densities, the integral of active LFA-1 is high because there is an overproduction of active LFA-1 beyond that needed for arrest. These molecules can accumulate because it takes some time for the cell to arrest even at a high level of activation. At the lowest chemokine densities, there is a period of time where the number of active integrin molecules in the contact zone is too low and the cell cannot bind firmly, but the total number of active integrins continues to accumulate. The net result is that there is a minimum in the integral of active LFA-1 at an intermediate IL-8 density. A further detailed mathematical explanation of this possibility is presented in Appendix A.

We have explored various metrics to understand the timescale of cell arrest, including the total number of active integrins on the cell and the integral of the number of chemokine bonds over rolling time. Theses quantities did not correlate with the time to stop. Instead, we find that the best indicator of the time it takes a cell to stop is the time for the first integrin molecule to become active. The correlation can be seen in Fig. 5 *B*. It was previously discussed that the time to stop approaches a minimum as the chemokine density increases (Fig. 3 *B*). This idea is mirrored in the time to first integrin activation. Even though IL-8 binding may initiate a signal very quickly when the IL-8 density is high, the signal still must propagate through the signal transduction network. The speed of this propagation is limited by the components of the cascade. Thus there is a lower limit for the time for the first integrin to be activated. At low chemokine density, the time for the first integrin to be activated suggests the rate at which individual microvilli will receive a sufficient signal. Because the number of activated microvilli is low, each active microvillus contributes essentially the same to the probability of firm adhesion, thus the linear correlation of time to first integrin activation and time to stop at low IL-8 densities.

Effect of signaling network

Next we explore the effects of parameters within the signaling cascade, keeping the chemokine density constant. We focus on parameters involving the Effector molecule because it represents an ill-defined part of the pathway.

Active Effector-$G_{\beta\gamma}$ dissociation

After an active $G_{\beta\gamma}$ subunit binds to an Effector molecule and activates it, the active Effector must dissociate and diffuse away to bind to and activate an integrin molecule. Thus, the dissociation rate of an active Effector molecule and a $G_{\beta\gamma}$ subunit (rate 13 in Table 2) affects how quickly the initial signal can lead to integrin activation and adhesion.

As expected, when active Effector dissociates more slowly from the $G_{\beta\gamma}$ subunit, the cell takes longer to firmly adhere, as shown in Fig. 6 *A*. At very fast dissociation rates, stop times approach a minimum as other steps in the signaling cascade limit the speed of activation. Also, the time to activate the first integrin again correlates well with the time to firm adhesion. The number of active integrin molecules available to bind and the number bound at the

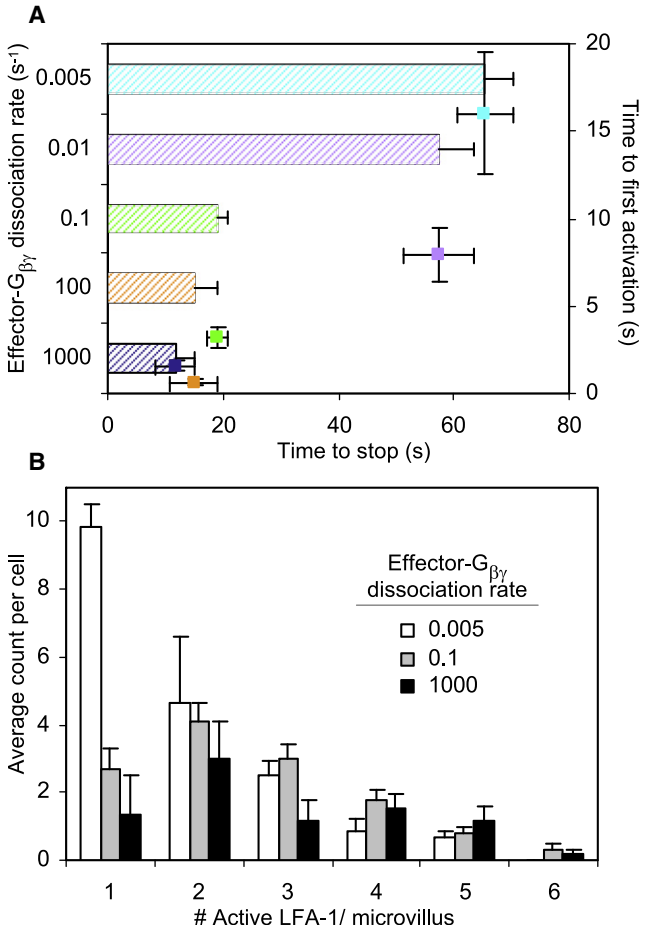

FIGURE 6 Changes in the active Effector-$G_{\beta\gamma}$ dissociation rate. (*A*) Time to stop and time to first activation. The average time to stop for each value of the active Effector-$G_{\beta\gamma}$ dissociation rate is plotted as a bar graph. The average time to the first activation as a function of the average time to stop is also included, with each colored symbol corresponding to the dissociation rate value of the same color. The faster integrin activation afforded by a faster dissociation rate results in a shorter time to stop. The time to the first active integrin correlates well with the time to stop. (*B*) A histogram of the number of active integrin molecules per microvillus at the stoppage point for different values of the dissociation rate. At the lowest dissociation rate, integrin activation is slow and there are many microvilli with a small number of active integrins. At faster dissociation rates and faster activation, the most probable and average active integrin density per microvillus increases. The total numbers of active microvilli represented are 18.5, 12.7, and 8.3 in the three cases, respectively.

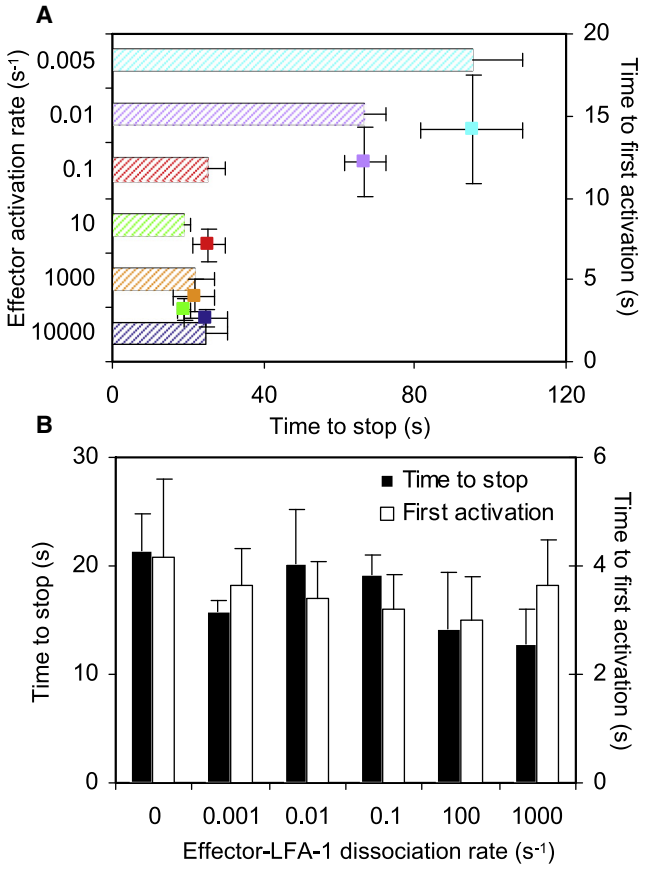

FIGURE 7 Time to stop and time to first activation for different signaling rates. (*A*) Changes in the Effector activation rate. When the Effector activation rate is small, integrin activation is slower, which correlates with the time to stop. (*B*) Changes in active Effector-LFA-1 dissociation rate. Neither the time to stop nor the time to first activation significantly vary with large changes in the dissociation rate, indicating that activation propagation by a single active Effector is not a crucial process in this model.

point of stopping are relatively constant for all active Effector-$G_{\beta\gamma}$ dissociation rates (data not shown). Unlike when the IL-8 density was varied, the total amount of activated integrin at the point of arrest is the same at all dissociation rates. When varying the Effector-$G_{\beta\gamma}$ dissociation rate, the input (IL-8) is the same, but the transduction to the integrin is different. Thus, it is the rate of LFA-1 activation in each microvillus that differs, resulting in a distribution of the level of activation per microvillus that depends on the intracellular signaling rate. The distributions at the point of arrest for various dissociation rates are shown in Fig. 6 *B*. At lower dissociation rates, the intracellular signaling is slower and therefore there are more microvilli that have low numbers of active integrin molecules on them. Because adhesion probability increases greatly when adhesion molecules are clustered, the slower-activating cells must roll longer before they have enough microvilli with a high enough level of active integrin to achieve firm adhesion. Because of this effect, the total number of active LFA-1 molecules on cells at the point of arrest is relatively constant, with the lower intracellular signaling rates having more active microvilli, but with fewer active LFA-1 per microvillus on average. At higher active Effector-$G_{\beta\gamma}$ dissociation rates, the distribution of active integrins per microvillus increases to an average value of 2.84 $\pm$ 0.2 (compared to 2.60 $\pm$ 0.12 at the base case). Correspondingly, cells stop slightly faster than at the base case dissociation rate (Fig. 6 *A*).

Effector activation

We also examined the effects of varying the rate at which an Effector molecule becomes active when bound to an active $G_{\beta\gamma}$ molecule (rate 17 in Table 2), as seen in Fig. 7 *A*.

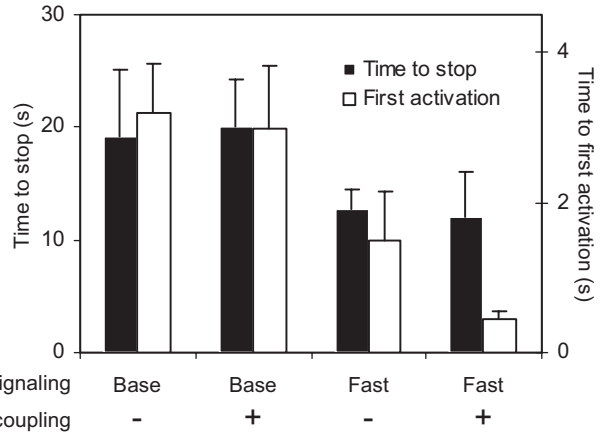

FIGURE 8 Time to stop and time to first activation with and without G–protein precoupling to the chemokine receptor. For both the base case parameters and a set of parameters that allowed faster intracellular signaling, the average time to stop and time to the first activation are shown. These quantities are also shown when the simulation was initiated with some G-protein and CXCR1 precoupled. There is no notable difference for the base case parameters, but with faster intracellular signaling, precoupling further decreased the time to the first activation.

When this rate is small, the intracellular signaling process is slow and leads to longer periods of rolling before firm adhesion, as anticipated. Again, slower steps in the signaling cascade limit the overall speed of integrin activation, resulting in a lower limit to the time to firm adhesion for fast Effector activation rates.

Active Effector-active LFA-1 dissociation

Additionally, we explored the rate of active Effector dissociation from active integrin (rates 14 and 15 in Table 2) in Fig. 7 *B*. Once an Effector molecule binds to and activates an integrin, it can dissociate from the integrin and go on to activate another integrin. However, an active integrin without a bound Effector may deactivate. The net effect is that the rate of active Effector dissociation from active LFA-1 did not have a significant effect on the time to stop. Even when active Effector was not allowed to dissociate from an active integrin, the time to stop did not increase because that integrin remained active and other Effector molecules in the microvillus were available to pass along the signal. When the dissociation rate was fast, the number of active integrins on a microvillus rapidly increased, but the time to stop was still limited by the contact time between the active microvilli and the adhesive surface. Although some deactivation did occur, it was not integrin deactivation due to Effector dissociation that limited the time to stop, because setting the integrin deactivation rate to zero did not change the results (data not shown).

G-protein precoupling

With this model, we were able to examine potential benefits of G-protein precoupling with the chemokine receptor so it is ready to be activated as soon as chemokine binds. To study this, we initialized the simulations with a number of G-protein molecules already bound to CXCR1 at the microvillus tip. The number of precoupled G-proteins in a given microvillus was chosen randomly from a uniform distribution from zero to the maximum possible. Our findings are presented in Fig. 8. We found that G-protein precoupling does not speed up cell arrest, most likely because other steps in the cascade are limiting.

Effect of external parameters

Finally, we investigated the effect that easily adjustable experimental parameters could have on the dynamics of firm adhesion at a constant IL-8 density of 220 sites/μm^2. These parameters were P-selectin density, ICAM-1 density, and shear rate. Fig. 9 *A* shows that, as long as there is some selectin present, the time to stop does not significantly change as selectin density increases. However, the distance rolled until firm adhesion decreases, corresponding to the rolling velocity decreasing with increasing selectin density. Because a similar number of active integrin bonds is required for arrest under all selectin densities tested (Fig. 9 *B*), cells must roll approximately the same time to achieve this level of activation before stopping. The total number of active integrins does increase with increasing selectin density. At lower selectin densities when cells are rolling more quickly, each chemokine bond will not persist as long. This decreases the opportunity for an active CXCR1 to activate a G-protein. Therefore, as seen in Fig. 9 *C*, fewer microvilli are activated for lower selectin densities, but each activated microvillus displays the same level of integrin activation, which ultimately allows firm adhesion with a small number of fully active microvilli. In the absence of selectin, the rolling velocity is significantly larger than when some selectin is present (38 μm/s vs. 16–5.2 μm/s), with only integrin interactions to slow the cell (unactivated β_2-integrins support rolling on ICAM-1). At this large velocity, microvilli are activated slowly, leading to a longer time before firm adhesion (Fig. 9 *A*).

Interestingly, increasing the ICAM-1 density does not affect the time to arrest, because a similar number of active integrins are bound at the point of firm adhesion under all ICAM-1 densities (Fig. 10 *A*). The number of active LFA-1 molecules on the cell is limiting in this case. The distance to stop, however, decreases with increasing ICAM-1 density, because of differences in rolling velocity. With higher ICAM-1 densities, resting LFA-1 bonds contribute to slow the rolling velocity, as illustrated by the 1-s average velocity as a function of time in Fig. 10 *B*, in which the cells roll slowly from the beginning of the simulation, before integrins are activated.

We also tested the effect of shear rate on the transition from rolling to firm adhesion. As seen in Fig. 11, cells roll for longer times and distances before stopping when exposed to higher shear rates. At higher shear rates, more active LFA-1

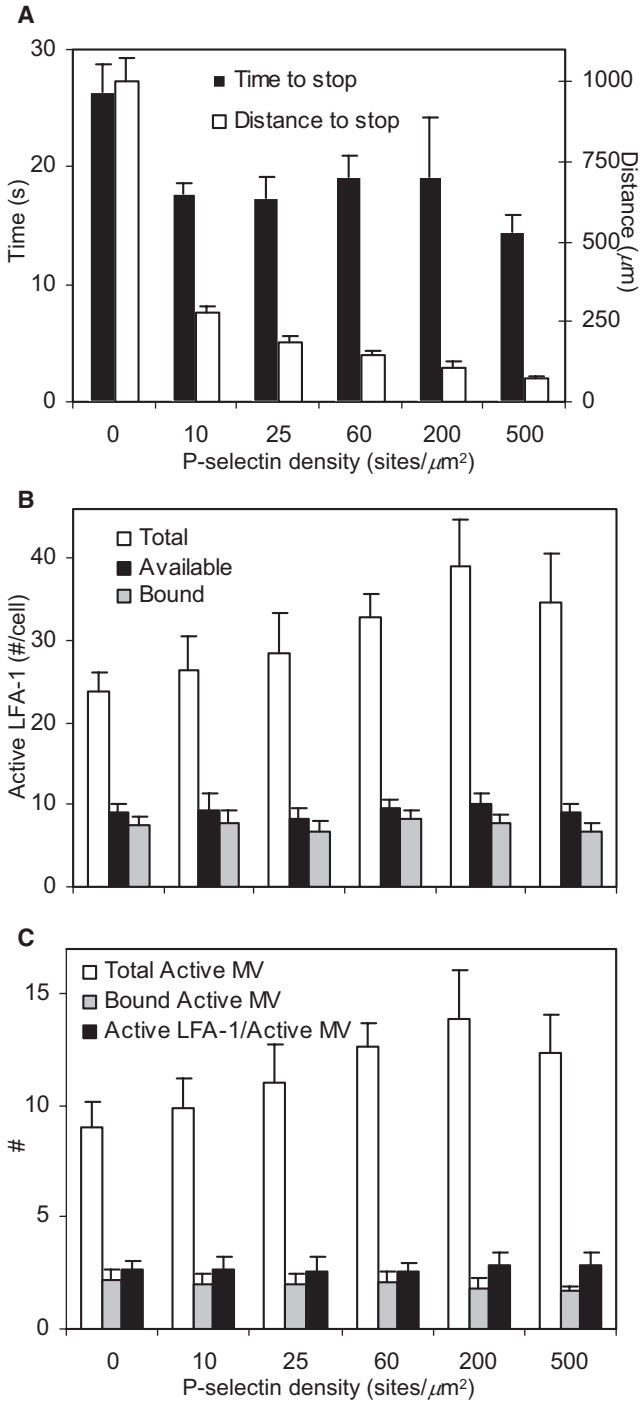

FIGURE 9 Effect of P–selectin density on the transition to firm adhesion. (*A*) Time and distance rolled before stopping on various P-selectin densities. As long as selectin is present, time to stop does not vary, however the distance to stop depends on the rolling velocity at the various selectin densities. (*B*) Average number of active LFA-1 molecules per cell at the point of firm adhesion. The total number of active LFA-1 molecules on the entire cell surface increases somewhat with selectin density whereas the number available to bind and bound on stopping remains relatively constant. (*C*) Average number of active microvilli at per cell at the point of firm adhesion. The total number of microvilli with any active integrins slightly increases as the selectin densities increases. However, the number of active microvilli bound on stopping does not significantly change.

bonds are required for the cell to stop, and it takes longer to reach that level of activation. Additionally, when cells are moving quickly at high shear rates, chemokine bonds do not last as long, so there is less time for the signal to be activated intracellularly where it can propagate and the rate of activation is slightly slower. This effect is small; the requirement of a larger number of active integrin bonds for cells to stop at higher shear rates is the main reason for the increase in the time to stop.

DISCUSSION

There are several mechanisms by which leukocytes may become activated to firmly adhere after a period of rolling at sites of inflammation. Some experiments suggest that selectin ligation during rolling serves also to signal integrin activation in the cell (60–62). Our lab previously recreated the transition from rolling to firm adhesion in an ISAD model by incorporating a MAPK signaling cascade into the cell. The activating signal was initiated by PSGL-1 on the cell surface binding to E-selectin (25,32). Another commonly shown method of cell activation is through exposure to inflammatory chemokines that bind to GPCRs on the cell (14,17–19,63). On release from endothelial cells, chemokine molecules have been shown to bind to glycosaminoglycans on the endothelial surface for juxtacrine presentation to rolling neutrophils (64,65). In this study, we focused on chemokine-mediated neutrophil activation through a G-protein signaling cascade.

We have extended previous Adhesive Dynamics models of cell rolling via selectin bonds to include the transition to firm adhesion. To simulate the transition from rolling to firm adhesion, we incorporated a signaling cascade that takes an initial extracellular chemokine signal and transforms it intracellularly through G-proteins to activate high-affinity integrin molecules on the cell surface. This ISAD model successfully recreated the transition from rolling to firm adhesion and was used to explore the effects of components of the signaling network on the dynamics of adhesion, as well as the effect of easily adjustable parameters on the time to become firmly bound.

Our simulations showed that, as cells rolled, they accumulated signal that resulted in a gradual increase in the number of active LFA-1 molecules on the cell. With the presence of high-affinity integrin bonds, cells began to exhibit longer pauses while rolling, followed by firm adhesion. When exposed to larger densities of chemokine on the adhesive surface, cells stopped more quickly, an observation also made in vitro by DiVietro et al. (18). Although larger chemokine densities resulted in more active integrins on the cell surface at the time of firm binding, the number of active

Each active microvillus is activated to the same degree, on average, as indicated by a constant number of active LFA-1 molecules per active microvillus.

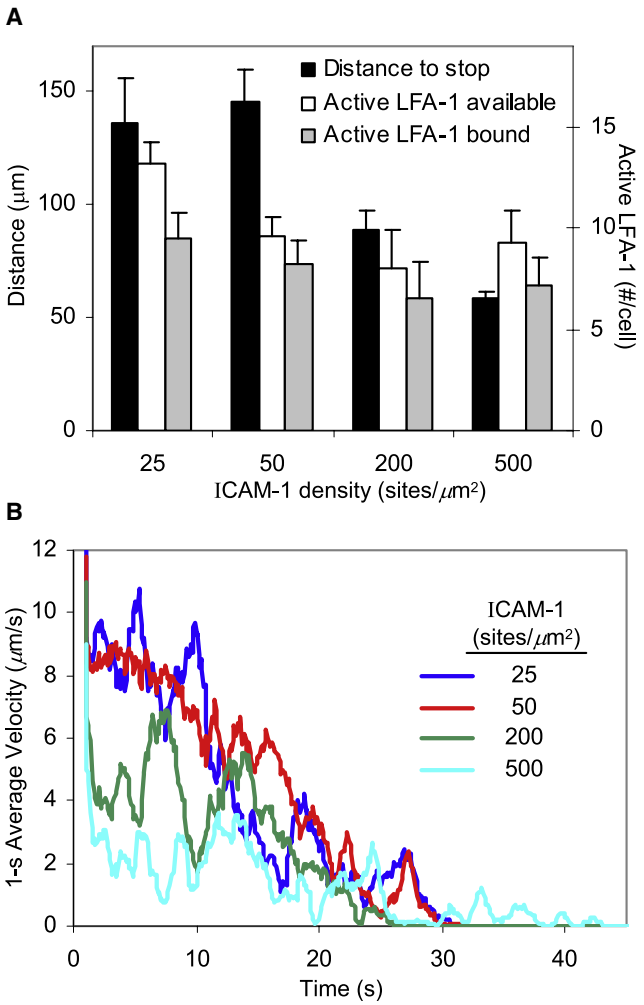

FIGURE 10 Effect of ICAM-1 density on the transition to firm adhesion. (*A*) Average distance to stop and number of active LFA-1 molecules per cell at various ICAM-1 densities. The distance rolled before firm adhesion decreases with increasing ICAM-1 densities because the rolling velocity decreases. The average number of active LFA-1 molecules available to bind and bound when the cell becomes firmly adherent do not significantly vary, suggesting that the number of active LFA-1 molecules on the cell is limiting for firm adhesion. (*B*) Average 1-s average velocity as a function of time for all cells at each ICAM-1 density tested. The average velocity over the previous 1 s was found for each cell as a function of time and the results were averaged for each set of conditions. At higher ICAM-1 densities, the cells roll more slowly starting at the beginning of the simulation, indicating that resting LFA-1 interactions are slowing the cells. These cells roll shorter distances, yet stop in about the same amount of time as cells exposed to lower ICAM-1 densities.

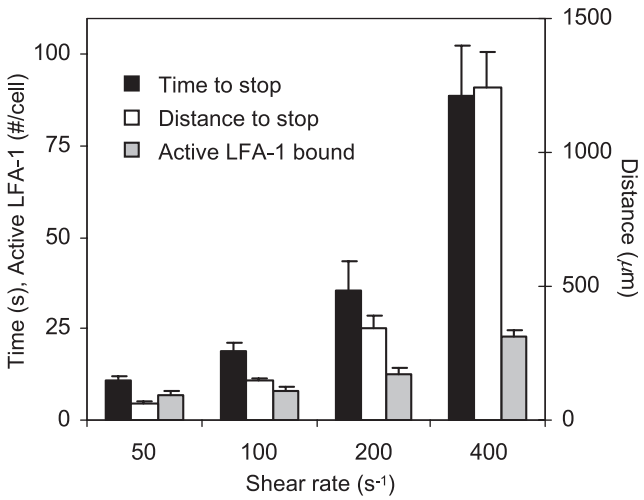

FIGURE 11 Effect of shear rate on the transition to firm adhesion. The time and distance rolled before stopping and the number of active LFA-1 bonds during firm adhesion are plotted for various shear rates. All quantities increase with shear rate. More active integrin bonds are required for stopping at the higher shear rates because of the larger force of flow, and it takes more time to reach the required level of activation. The time to stop increases more rapidly than the number of active integrins required, indicating that the rate of activation decreases slightly as shear rate increases due to the limited persistence time of the chemokine bonds during the faster rolling.

integrin bonds at the point of firm adhesion was relatively constant. Our results are consistent with the experimental observations of DiVietro et al. (18); furthermore, we predict that densities of IL-8 higher than in the experiments would not change the time to stop, but lower densities than they used would further increase the time to stop (Fig. 3). We assessed the effect of external parameters on the transition to firm adhesion as well. Neither selectin density nor ICAM-1 density dramatically changed the rolling time before firm adhesion, although they did affect the distance rolled because they altered the rolling velocity. Because the number of active LFA-1 bonds required for firm adhesion increases as shear rate increases, the time before firm adhesion also increases. This time is required for the cell to accumulate more active LFA-1 molecules.

We noted that the timescale to activate one integrin molecule correlated with the time it took the cells to ultimately stop. Changing reaction rates within the signaling cascade also affected the time to stop in accord with the resulting timescale for integrin activation. Furthermore, these simulations that varied the speed of intracellular signaling suggested a role for integrin clustering in firm adhesion. With slower active Effector dissociation from the $G_{\beta\gamma}$ subunit or a slower Effector activation rate, intracellular signaling is consequently slower and cells take longer to become adherent. However, changes in the rate of active Effector dissociation from active LFA-1 did not have a significant effect on the time to stop. We also found that G-protein precoupling with CXCR1 could contribute to faster activation only if the remainder of the signaling cascade was fast. This indicates that scaffolding many of the components of the signaling cascade near the site of initial activation could speed up integrin activation and the onset of firm adhesion.

We also considered the effects of two pharmacological treatments of G-protein networks that are typically carried out. One is to use a toxin, such as pertussis toxin; this would have destroyed the G-protein activity, and there would have been no adhesion at all. The second is to use a nonhydrolyzable GTP, such as GTPγS. GTPγS would prevent

G_α deactivation and hence the reassembly of the G-protein, which prevents deactivation of $G_{\beta\gamma}$. We carried out simulations in which the G_α deactivation rate was zero to model the effect of GTPγS (data not shown). They indicated little effect on the time to stop, suggesting that the $G_{\beta\gamma}$ deactivation rate, which includes G_α deactivation and subsequent recombination with $G_{\beta\gamma}$, is already slow in this model.

In the base case simulations, a rolling cell generally stopped on the order of tens of seconds, with integrins becoming active on the order of a second. When parameter changes were made such that the integrins on a chemokine-activated microvillus became active very quickly, this increase in activation was not manifested in the time to stop. Because of the morphological simplifications of this model, it is highly unlikely for a microvillus to become active and then firmly adhere during the same visit to the contact area. Instead, adhesion of active integrins occurs on reentry into the contact area after a full cell rotation. This prevented some potential benefits of fast activation from being observed. Still, it is possible that fast activation can indeed lead to faster firm binding, which some changes in the model could reveal. If activation was not as local as to be restricted to the microvillus in which it was initiated, integrins could be activated further from a chemokine binding site. Activation occurring at the leading edge of the contact zone, then, could make more rapid firm adhesion possible.

With a hard sphere model for the cell, only molecules located on the microvillus tips can reach and bind to the surface. Therefore, we model only those integrins that might be located on the microvillus tips assuming a uniform distribution of integrins on the cell surface. We showed in this and previous work that clustering on the microvillus tips can contribute to stronger adhesion (27). However, it is possible that integrin molecules tend to be on the cell body rather than the microvilli (66,67), with deformability of the cell surface and membrane unwrinkling allowing these molecules to contact the vessel wall (68,69). Simulation results would change if the integrin molecules were not located on the microvillus tips, but this assumption may approximate other features of the cell adhesion process. For example, ICAM-1 molecules are preferentially located on endothelial microvilli (13), which could facilitate adhesion to endothelial cells much like integrin localization to neutrophil microvilli. As further validation, it has been proposed that besides an increase in integrin affinity for ICAM-1, the integrins may cluster on activation (70–74). By localizing integrins to the neutrophil microvilli in this model, we are effectively clustering them, which contributes to the achievement of firm adhesion. Further, one can include other β_2-integrins, such as Mac-1, although we suspect these molecules are upregulated too slowly to affect the initial arrest of the leukocyte.

We previously modeled cell activation via the PSGL-1/E-selectin-mediated MAPK pathway using a similar method (25). Although an in-depth comparison between this model and the previous model (25) is not possible due to the increased detail in the current work, we can compare some trends. Both models showed a gradual increase in the number of active integrins on the cell as the cells rolled. Furthermore, increasing the rate of activation resulted in a shorter rolling time before stopping in both models. In addition, the time to stop approached a minimum for fast activation rates. Increasing E-selectin density, which provided the signal when bound to PSGL-1 in the previous model, resulted in a faster time to arrest (25). Similarly, increasing the IL-8 signal in this model allowed the cell to stop more quickly (Fig. 3). Changes in ICAM-1 density, however, gave different results. In the previous model (25), increasing the ICAM-1 density led to a faster time to arrest, whereas ICAM-1 density affected the distance to stop, but did not significantly affect the time to stop in this model (Fig. 10). The difference may be due to the number of integrin molecules on each microvillus in the models. In this study, the number of LFA-1 on the cell is small and likely limiting, but it is significantly larger in the previous work (25). In a neutrophil, it is possible that both the selectin-mediated MAPK pathway and the chemokine-mediated G-protein pathway are acting simultaneously; thus synergism between two or more pathways could be incorporated into the model. There is potential to use a model like this to examine alternative activation pathways, perhaps to predict which is dominant in a given situation. As more details regarding activation networks within neutrophils emerge, they can be easily incorporated in an ISAD model.

A basic difference between the two models, however, is how adhesion and signaling are coupled. In the MAPK simulations (25), the adhesion molecule supporting rolling also generated a signal. In this study, the chemokine receptor generates a signal with limited adhesive function, and an additional molecule (PSGL-1) supports rolling adhesion. In both models, signaling results in integrin conformational change. However, neither model incorporates a force-dependent change in the adhesive function or signal sensitivity of the adhesion molecules themselves. This may be an oversimplification, because Alon and Ley (75) have speculated that adhesive force can ''prime'' an adhesion molecule and make it more susceptible to activation. Because conformational changes in adhesion molecules are downstream of signaling and because signaling and rolling adhesion are uncoupled in both of our models, we do not believe there is any fundamental difference in how the two systems activate integrin-mediated adhesion. Rather, the differences are restricted only to differences in the topology of the signaling network and the concentration of its constituents.

It should also be noted that an important future use of these simulations is to examine lymphocyte activation. Lymphocytes use multiple chemokine receptors and their ligands to identify sites of homing. The combination of chemokine identity and density lead to integrated signals that can activate integrins, stimulate adhesion, and dictate

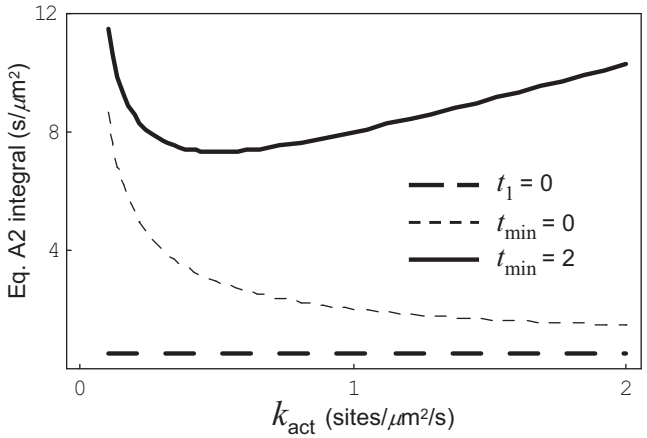

FIGURE 12 Theoretical active integrin integrals as a function of activation rate. The integral in Eq. A2 is plotted as a function of activation rate for various forms of the minimum adhesion time, t_1. When $t_1 = 0$ s, k_{ad} is a linear function of ρ and the integral is constant as mentioned in the text. When t_1 is nonzero as in Eq. A5, the integral is no longer constant. Introducing a t_{min} generates a minimum in the integral. For this simple demonstration, $k_{on} = 1\ \mu m^2/s$ and $\rho_0 = 1$ site/μm^2.

homing patterns (75). We will address this integration in future work.

APPENDIX A

Analytic Model For Stopping

As noted in Fig. 5 *A*, the integral of active LFA-1 over rolling time is relatively constant, but has a slight minimum as IL-8 density varies. The idea that both the number of active integrins and contact time with the adhesive surface contribute to the time it takes a cell to stop can be modeled in a way similar to dynamic force spectroscopy experiments, where the probability of bond breakage depends on the rate of dissociation for the bond and the probability that it has not yet broken (76–78). Here, the probability that a cell will firmly adhere in a small time (t, $t + dt$) is equal to the cellular association rate, k_{ad}, multiplied by the probability that the cell did not yet firmly bind. Assuming the cellular association rate depends on the adhesion molecule density, ρ, this leads to a probability of binding:

$$P_{ad}(\rho, t) = k_{ad}(\rho(t)) \times \exp\left[-\int_0^t k_{ad}\left(\rho\left(t'\right)\right)dt'\right]. \quad \text{(A1)}$$

The most probable time to stop, t^*, is found when $\partial P_{ad}/\partial t = 0$. Thus, the integral of active integrin density over time to the stop point in the simulations can be estimated by:

$$\int_0^{t^*} \rho\left(t'\right)dt'. \quad \text{(A2)}$$

For simplicity, we make the approximation that the active integrin density is a linear function of time with rate constant k_{act}:

$$\rho(t) = k_{act}t. \quad \text{(A3)}$$

If the adhesion rate k_{ad} is a linear function of ρ, then it turns out that the integral in Eq. A2 is constant with respect to k_{act}. However, a slightly different form for k_{ad} may be appropriate. If k_{ad} is zero up to a minimum time t_1, then increases linearly with active integrin density:

$$k_{ad}(t) = \begin{cases} 0 & , t \le t_1 \\ k_{on}(\rho(t) - \rho(t_1)) & , t > t_1 \end{cases}, \quad \text{(A4)}$$

the integral in Eq. A2 is no longer constant. Consider the case when the minimum adhesion time, t_1, decreases with the activation rate, k_{act}, to some nonzero minimum, t_{min}. This could be described by:

$$t_1 = t_{min} + \rho_0 k_{act}^{-1}. \quad \text{(A5)}$$

It is reasonable that the minimum adhesion time itself has a minimum for this model because an activated microvillus must reenter the contact zone before having a chance to firmly bind. Furthermore, if a minimum number of active integrins is required for firm adhesion, the minimum adhesion time should decrease as the activation rate increases. With such a model for t_1, Fig. 12 shows that the integral in Eq. A2 reaches a minimum as a function of activation rate. Clearly, the adhesion rates are more complicated than the simple approximations here, but this provides a possible explanation for the minimum in the active integrin integral over rolling time (Fig. 5 *A*) as the activation rate changes for different IL-8 densities.

The authors are grateful for support from the National Institutes of Health (HL18208) and the National Science Foundation through a Graduate Research Fellowship to K.E.C.

REFERENCES

1. Hentzen, E. R., S. Neelamegham, G. S. Kansas, J. A. Benanti, L. V. McIntire, et al. 2000. Sequential binding of CD11a/CD18 and CD11b/CD18 defines neutrophil capture and stable adhesion to intercellular adhesion molecule-1. *Blood*. 95:911–920.
2. Green, C. E., U. Y. Schaff, M. R. Sarantos, A. F. Lum, D. E. Staunton, et al. 2006. Dynamic shifts in LFA-1 affinity regulate neutrophil rolling, arrest, and transmigration on inflamed endothelium. *Blood*. 107: 2101–2111.
3. Salas, A., M. Shimaoka, U. Phan, M. Kim, and T. A. Springer. 2006. Transition from rolling to firm adhesion can be mimicked by extension of integrin alphaLbeta2 in an intermediate affinity state. *J. Biol. Chem.* 281:10876–10882.
4. Sarantos, M. R., S. Raychaudhuri, A. F. Lum, D. E. Staunton, and S. I. Simon. 2005. Leukocyte function-associated antigen 1-mediated adhesion stability is dynamically regulated through affinity and valency during bond formation with intercellular adhesion molecule-1. *J. Biol. Chem.* 280:28290–28298.
5. Takagi, J., B. M. Petre, T. Walz, and T. A. Springer. 2002. Global conformational rearrangements in integrin extracellular domains in outside-in and inside-out signaling. *Cell*. 110:599–611.
6. Shimaoka, M., J. Takagi, and T. A. Springer. 2002. Conformational regulation of integrin structure and function. *Annu. Rev. Biophys. Biomol. Struct.* 31:485–516.
7. Shimaoka, M., C. Lu, R. T. Palframan, U. H. von Andrian, A. McCormack, et al. 2001. Reversibly locking a protein fold in an active conformation with a disulfide bond: integrin alphaL I domains with high affinity and antagonist activity in vivo. *Proc. Natl. Acad. Sci. USA*. 98:6009–6014.
8. Shimaoka, M., T. Xiao, J. H. Liu, Y. Yang, Y. Dong, et al. 2003. Structures of the alpha L I domain and its complex with ICAM-1 reveal a shape-shifting pathway for integrin regulation. *Cell*. 112:99–111.
9. Dransfield, I., C. Cabanas, A. Craig, and N. Hogg. 1992. Divalent cation regulation of the function of the leukocyte integrin LFA-1. *J. Cell Biol.* 116:219–226.
10. Labadia, M. E., D. D. Jeanfavre, G. O. Caviness, and M. M. Morelock. 1998. Molecular regulation of the interaction between leukocyte

function-associated antigen-1 and soluble ICAM-1 by divalent metal cations. *J. Immunol.* 161:836–842.

11. Lu, C., M. Shimaoka, M. Ferzly, C. Oxvig, J. Takagi, et al. 2001. An isolated, surface-expressed I domain of the integrin alphaLbeta2 is sufficient for strong adhesive function when locked in the open conformation with a disulfide bond. *Proc. Natl. Acad. Sci. USA.* 98:2387–2392.
12. Andrew, D., A. Shock, E. Ball, S. Ortlepp, J. Bell, et al. 1993. KIM185, a monoclonal antibody to CD18 which induces a change in the conformation of CD18 and promotes both LFA-1- and CR3-dependent adhesion. *Eur. J. Immunol.* 23:2217–2222.
13. Simon, S. I., and C. E. Green. 2005. Molecular mechanics and dynamics of leukocyte recruitment during inflammation. *Annu. Rev. Biomed. Eng.* 7:151–185.
14. Campbell, J. J., J. Hedrick, A. Zlotnik, M. A. Siani, D. A. Thompson, et al. 1998. Chemokines and the arrest of lymphocytes rolling under flow conditions. *Science.* 279:381–384.
15. Tangemann, K., M. D. Gunn, P. Giblin, and S. D. Rosen. 1998. A high endothelial cell-derived chemokine induces rapid, efficient, and subset-selective arrest of rolling T lymphocytes on a reconstituted endothelial substrate. *J. Immunol.* 161:6330–6337.
16. Gerszten, R. E., E. A. Garcia-Zepeda, Y. C. Lim, M. Yoshida, H. A. Ding, et al. 1999. MCP-1 and IL-8 trigger firm adhesion of monocytes to vascular endothelium under flow conditions. *Nature.* 398:718–723.
17. Seo, S. M., L. V. McIntire, and C. W. Smith. 2001. Effects of IL-8, Gro-alpha, and LTB(4) on the adhesive kinetics of LFA-1 and Mac-1 on human neutrophils. *Am. J. Physiol. Cell Physiol.* 281:C1568–C1578.
18. DiVietro, J. A., M. J. Smith, B. R. Smith, L. Petruzzelli, R. S. Larson, et al. 2001. Immobilized IL-8 triggers progressive activation of neutrophils rolling in vitro on P-selectin and intercellular adhesion molecule-1. *J. Immunol.* 167:4017–4025.
19. Rainger, G. E., A. C. Fisher, and G. B. Nash. 1997. Endothelial-borne platelet-activating factor and interleukin-8 rapidly immobilize rolling neutrophils. *Am. J. Physiol.* 272:H114–H122.
20. Shamri, R., V. Grabovsky, J. M. Gauguet, S. Feigelson, E. Manevich, et al. 2005. Lymphocyte arrest requires instantaneous induction of an extended LFA-1 conformation mediated by endothelium-bound chemokines. *Nat. Immunol.* 6:497–506.
21. Gopalan, P. K., A. R. Burns, S. I. Simon, S. Sparks, L. V. McIntire, et al. 2000. Preferential sites for stationary adhesion of neutrophils to cytokine-stimulated HUVEC under flow conditions. *J. Leukoc. Biol.* 68:47–57.
22. Hammer, D. A., and S. M. Apte. 1992. Simulation of cell rolling and adhesion on surfaces in shear flow: general results and analysis of selectin-mediated neutrophil adhesion. *Biophys. J.* 63:35–57.
23. Chang, K. C., D. F. Tees, and D. A. Hammer. 2000. The state diagram for cell adhesion under flow: leukocyte rolling and firm adhesion. *Proc. Natl. Acad. Sci. USA.* 97:11262–11267.
24. Bhatia, S. K., M. R. King, and D. A. Hammer. 2003. The state diagram for cell adhesion mediated by two receptors. *Biophys. J.* 84:2671–2690.
25. Krasik, E. F., K. E. Caputo, and D. A. Hammer. 2008. Adhesive dynamics simulation of neutrophil arrest with stochastic activation. *Biophys. J.* 95:1716–1728.
26. King, M. R., and D. A. Hammer. 2001. Multiparticle adhesive dynamics: hydrodynamic recruitment of rolling leukocytes. *Proc. Natl. Acad. Sci. USA.* 98:14919–14924.
27. Caputo, K. E., and D. A. Hammer. 2005. Effect of microvillus deformability on leukocyte adhesion explored using adhesive dynamics simulations. *Biophys. J.* 89:187–200.
28. Caputo, K. E., D. Lee, M. R. King, and D. A. Hammer. 2007. Adhesive dynamics simulations of the shear threshold effect for leukocytes. *Biophys. J.* 92:787–797.
29. Chang, K. C., and D. A. Hammer. 2000. Adhesive dynamics simulations of sialyl-Lewis(x)/E-selectin-mediated rolling in a cell-free system. *Biophys. J.* 79:1891–1902.
30. Kuo, S. C., D. A. Hammer, and D. A. Lauffenburger. 1997. Simulation of detachment of specifically bound particles from surfaces by shear flow. *Biophys. J.* 73:517–531.
31. Ward, M. D., M. Dembo, and D. A. Hammer. 1994. Kinetics of cell detachment: peeling of discrete receptor clusters. *Biophys. J.* 67:2522–2534.
32. Krasik, E. F., K. L. Yee, and D. A. Hammer. 2006. Adhesive dynamics simulation of neutrophil arrest with deterministic activation. *Biophys. J.* 91:1145–1155.
33. Murdoch, C., and A. Finn. 2000. Chemokine receptors and their role in inflammation and infectious diseases. *Blood.* 95:3032–3043.
34. Moore, K. L., A. Varki, and R. P. McEver. 1991. GMP-140 binds to a glycoprotein receptor on human neutrophils: evidence for a lectin-like interaction. *J. Cell Biol.* 112:491–499.
35. Rodgers, S. D., R. T. Camphausen, and D. A. Hammer. 2000. Sialyl Lewis(x)-mediated, PSGL-1-independent rolling adhesion on P-selectin. *Biophys. J.* 79:694–706.
36. Ushiyama, S., T. M. Laue, K. L. Moore, H. P. Erickson, and R. P. McEver. 1993. Structural and functional characterization of monomeric soluble P-selectin and comparison with membrane P-selectin. *J. Biol. Chem.* 268:15229–15237.
37. Norman, K. E., A. G. Katopodis, G. Thoma, F. Kolbinger, A. E. Hicks, et al. 2000. P-selectin glycoprotein ligand-1 supports rolling on E- and P-selectin in vivo. *Blood.* 96:3585–3591.
38. Shao, J. Y., H. P. Ting-Beall, and R. M. Hochmuth. 1998. Static and dynamic lengths of neutrophil microvilli. *Proc. Natl. Acad. Sci. USA.* 95:6797–6802.
39. Moser, B., C. Schumacher, V. von Tscharner, I. Clark-Lewis, and M. Baggiolini. 1991. Neutrophil-activating peptide 2 and gro/melanoma growth-stimulatory activity interact with neutrophil-activating peptide 1/interleukin 8 receptors on human neutrophils. *J. Biol. Chem.* 266:10666–10671.
40. Chang, K. C., and D. A. Hammer. 1999. The forward rate of binding of surface-tethered reactants: Effect of relative motion between two surfaces. *Biophys. J.* 76:1280–1292.
41. Dembo, M., D. C. Torney, K. Saxman, and D. Hammer. 1988. The reaction-limited kinetics of membrane-to-surface adhesion and detachment. *Proc. R. Soc. Lond. B. Biol. Sci.* 234:55–83.
42. Marshall, B. T., K. K. Sarangapani, J. Wu, M. B. Lawrence, R. P. McEver, et al. 2006. Measuring molecular elasticity by atomic force microscope cantilever fluctuations. *Biophys. J.* 90:681–692.
43. Fritz, J., A. G. Katopodis, F. Kolbinger, and D. Anselmetti. 1998. Force-mediated kinetics of single P-selectin/ligand complexes observed by atomic force microscopy. *Proc. Natl. Acad. Sci. USA.* 95: 12283–12288.
44. Staunton, D. E., M. L. Dustin, H. P. Erickson, and T. A. Springer. 1990. The arrangement of the immunoglobulin-like domains of ICAM-1 and the binding sites for LFA-1 and rhinovirus. *Cell.* 61:243–254.
45. Otaki, J. M., and S. Firestein. 2001. Length analyses of mammalian G-protein-coupled receptors. *J. Theor. Biol.* 211:77–100.
46. Clore, G. M., E. Appella, M. Yamada, K. Matsushima, and A. M. Gronenborn. 1990. Three-dimensional structure of interleukin 8 in solution. *Biochemistry.* 29:1689–1696.
47. Bell, G. I. 1978. Models for the specific adhesion of cells to cells. *Science.* 200:618–627.
48. Zhang, X., E. Wojcikiewicz, and V. T. Moy. 2002. Force spectroscopy of the leukocyte function-associated antigen-1/intercellular adhesion molecule-1 interaction. *Biophys. J.* 83:2270–2279.
49. Evans, E., A. Leung, V. Heinrich, and C. Zhu. 2004. Mechanical switching and coupling between two dissociation pathways in a P-selectin adhesion bond. *Proc. Natl. Acad. Sci. USA.* 101:11281–11286.
50. Alon, R., and A. Etzioni. 2003. LAD-III, a novel group of leukocyte integrin activation deficiencies. *Trends Immunol.* 24:561–566.
51. Thelen, M. 2001. Dancing to the tune of chemokines. *Nat. Immunol.* 2:129–134.

52. Neves, S. R., P. T. Ram, and R. Iyengar. 2002. G protein pathways. *Science*. 296:1636–1639.

53. Hamm, H. E. 1998. The many faces of G protein signaling. *J. Biol. Chem.* 273:669–672.

54. Kinashi, T. 2005. Intracellular signaling controlling integrin activation in lymphocytes. *Nat. Rev. Immunol.* 5:546–559.

55. Mor, A., M. L. Dustin, and M. R. Philips. 2007. Small GTPases and LFA-1 reciprocally modulate adhesion and signaling. *Immunol. Rev.* 218:114–125.

56. Mahama, P. A., and J. J. Linderman. 1994. A Monte Carlo study of the dynamics of G-protein activation. *Biophys. J.* 67:1345–1357.

57. Shea, L. D., R. R. Neubig, and J. J. Linderman. 2000. Timing is everything the role of kinetics in G protein activation. *Life Sci.* 68:647–658.

58. Shea, L. D., G. M. Omann, and J. J. Linderman. 1997. Calculation of diffusion-limited kinetics for the reactions in collision coupling and receptor cross-linking. *Biophys. J.* 73:2949–2959.

59. Kruk, P. J., H. Korn, and D. S. Faber. 1997. The effects of geometrical parameters on synaptic transmission: a Monte Carlo simulation study. *Biophys. J.* 73:2874–2890.

60. Simon, S. I., Y. Hu, D. Vestweber, and C. W. Smith. 2000. Neutrophil tethering on E-selectin activates beta 2 integrin binding to ICAM-1 through a mitogen-activated protein kinase signal transduction pathway. *J. Immunol.* 164:4348–4358.

61. Hentzen, E., D. McDonough, L. McIntire, C. W. Smith, H. L. Goldsmith, et al. 2002. Hydrodynamic shear and tethering through E-selectin signals phosphorylation of p38 MAP kinase and adhesion of human neutrophils. *Ann. Biomed. Eng.* 30:987–1001.

62. Smolen, J. E., T. K. Petersen, C. Koch, S. J. O'Keefe, W. A. Hanlon, et al. 2000. L-selectin signaling of neutrophil adhesion and degranulation involves p38 mitogen-activated protein kinase. *J. Biol. Chem.* 275:15876–15884.

63. Laudanna, C., and R. Alon. 2006. Right on the spot. Chemokine triggering of integrin-mediated arrest of rolling leukocytes. *Thromb. Haemost.* 95:5–11.

64. Middleton, J., S. Neil, J. Wintle, I. Clark-Lewis, H. Moore, et al. 1997. Transcytosis and surface presentation of IL-8 by venular endothelial cells. *Cell.* 91:385–395.

65. Middleton, J., A. M. Patterson, L. Gardner, C. Schmutz, and B. A. Ashton. 2002. Leukocyte extravasation: chemokine transport and presentation by the endothelium. *Blood.* 100:3853–3860.

66. Erlandsen, S. L., S. R. Hasslen, and R. D. Nelson. 1993. Detection and spatial distribution of the beta 2 integrin (Mac-1) and L-selectin (LECAM-1) adherence receptors on human neutrophils by high-resolution field emission SEM. *J. Histochem. Cytochem.* 41:327–333.

67. Berlin, C., R. F. Bargatze, J. J. Campbell, U. H. von Andrian, M. C. Szabo, et al. 1995. alpha 4 integrins mediate lymphocyte attachment and rolling under physiologic flow. *Cell.* 80:413–422.

68. Muller, W. A. 2002. Leukocyte-endothelial cell interactions in the inflammatory response. *Lab. Invest.* 82:521–533.

69. Dewitt, S., and M. Hallett. 2007. Leukocyte membrane ''expansion'': a central mechanism for leukocyte extravasation. *J. Leukoc. Biol.* 81:1160–1164.

70. van Kooyk, Y., S. J. van Vliet, and C. G. Figdor. 1999. The actin cytoskeleton regulates LFA-1 ligand binding through avidity rather than affinity changes. *J. Biol. Chem.* 274:26869–26877.

71. van Kooyk, Y., and C. G. Figdor. 2000. Avidity regulation of integrins: the driving force in leukocyte adhesion. *Curr. Opin. Cell Biol.* 12:542–547.

72. Lum, A. F., C. E. Green, G. R. Lee, D. E. Staunton, and S. I. Simon. 2002. Dynamic regulation of LFA-1 activation and neutrophil arrest on intercellular adhesion molecule 1 (ICAM-1) in shear flow. *J. Biol. Chem.* 277:20660–20670.

73. Alon, R., and S. Feigelson. 2002. From rolling to arrest on blood vessels: leukocyte tap dancing on endothelial integrin ligands and chemokines at sub-second contacts. *Semin. Immunol.* 14:93–104.

74. Hogg, N., R. Henderson, B. Leitinger, A. McDowall, J. Porter, et al. 2002. Mechanisms contributing to the activity of integrins on leukocytes. *Immunol. Rev.* 186:164–171.

75. Alon, R., and K. Ley. 2008. Cells on the run: shear-regulated integrin activation in leukocyte rolling and arrest on endothelial cells. *Curr. Opin. Cell Biol.* 20:525–532.

76. Evans, E. 1995. Physical actions in biological adhesion. *In* Structure and Dynamics of Membranes: Generic and Specific Interactions. R. Lipowsky and E. Sackmann, editors. Amsterdam: Elsevier Science. 723–753.

77. Evans, E., D. Berk, and A. Leung. 1991. Detachment of agglutinin-bonded red blood cells. I. Forces to rupture molecular-point attachments. *Biophys. J.* 59:838–848.

78. Evans, E., and K. Ritchie. 1997. Dynamic strength of molecular adhesion bonds. *Biophys. J.* 72:1541–1555.

79. Rinko, L. J., M. B. Lawrence, and W. H. Guilford. 2004. The molecular mechanics of P- and L-selectin lectin domains binding to PSGL-1. *Biophys. J.* 86:544–554.

80. Eniola, A. O., E. F. Krasik, L. A. Smith, G. Song, and D. A. Hammer. 2005. I-Domain of lymphocyte function-associated antigen-1 mediates rolling of polystyrene particles on ICAM-1 under flow. *Biophys. J.* 89:3577–3588.